CAUCHY – Jurnal Matematika Murni dan Aplikasi
Volume 11 (2) (2026), Pages 1932–1946
p-ISSN: 2086-0382; e-ISSN: 2477-3344

Numerical Solution of 2D Advection-Diffusion for River Pollutant Transport using the Finite Element Method

Muhamad Adzka Rizkia, Rahma Alya Zahrani, Zelisha Pitriatuz Zahra Fauzi, Foky Michelin, Najwaa Alifya Azka, Faiza Mayla Sabita, Mualim Arya Ilyas Wiradinata, Ferdy Aliansyah Hasyim, Mochamad Tito Julianto, Sri Nurdiati, Mohamad Khoirun Najib*, and Syukri Arif Rafhida

School of Data Science, Mathematics, and Informatics, IPB University, Bogor, Indonesia

Abstract

Pollutant dispersion in rivers is governed by advection, diffusion, and the physical characteristics of the channel. This paper models two-dimensional pollutant transport using the advection-diffusion equation and solves it numerically with the Finite Element Method (FEM) under five scenarios: constant flow with a single pollutant source, flow that follows a meandering channel, constant flow with two sources, the presence of a rock obstacle, and an irregular river domain. Simulations are implemented in Mathematica through domain construction, mesh generation, and a Finite Element-based numerical solution. The results show that flow velocity is the primary driver of plume movement, while diffusion smooths concentration gradients. Comparative analysis across the five scenarios demonstrates that the irregular domain produces the largest plume area among all cases, while multi-source, obstacle-containing, and irregular configurations each independently contribute to increased plume width and spatial complexity compared to the single-source straight-channel case. Physical obstacles and channel irregularities, as represented in the prescribed velocity field, produce wake-like retention patterns and plume deviation, illustrating more geometry-sensitive transport behavior than simplified channel models. These findings highlight the importance of geometry-aware flow representations for understanding river pollutant transport in numerical modelling studies.

Keywords: Advection-diffusion; Finite element method; Numerical simulation; Pollutant dispersion; River geometry

1. Introduction

Rivers are critical water resources that support ecological functions as well as social and economic activities [1–4]. However, human activities such as settlements [5], [6], agriculture [7], [8], and industry [9], [10] can discharge waste into rivers which can degrade water quality and reduce the river's ecological and economic functions. River water quality management is regulated in Indonesia under Government Regulation No. 82/2001 on water quality management and pollution control [11].

It is not possible to model rainfall-driven water movement and the substances it carries with 100% fidelity due to strong spatio-temporal variability and field uncertainties [12–15]; however, river flow and in-channel transport of water and dissolved pollutants can be modeled

*Corresponding author. E-mail: mkhoirun@apps.ipb.ac.id

Received: May 22, 2026 Revised: June 24, 2026 Accepted: August 17, 2026
DOI: https://doi.org/10.18860/cauchy.v11i2.42814

mathematically and numerically as a representative approximation. Once pollutants enter a river, their spatial-temporal evolution is mainly governed by transport and spreading processes. The bulk movement of contaminants along the flow is commonly described as advection, while their spreading from regions of high concentration to low concentration is described as diffusion (or dispersion). [16]. These mechanisms are commonly represented by the advection-diffusion equation, a partial differential equation (PDE) used to describe mass transport in fluids [17, 18]. Because the ADE depends on both space and time, it provides a continuous description of concentration changes as transport processes evolve.

In realistic field conditions, however, obtaining analytical solutions of the ADE is frequently impractical. River flow velocities may vary spatially, boundary conditions can be nonuniform, and the computational domain may be irregular due to natural geomorphology. Such complexities motivate the use of numerical approaches commonly applied in open-channel and environmental flow modeling [19]. Among numerical techniques, the Finite Element Method (FEM) is a strong candidate because it supports complex geometries and can provide stable and accurate approximations for flow-transport problems when formulated appropriately [20, 21].

Despite this, many pollutant-spread studies still rely on simplified assumptions such as straight river reaches, uniform widths, and constant flow velocity, which may not represent real river behavior adequately. For example, prior numerical works often consider regular domains and idealized flow conditions for tractability [22]. For instance, Alman [22] solved the 2D advection-diffusion equation using the Dufort-Frankel finite difference method but limited the domain to a straight channel geometry. Similiarly, Lee and Seo [23, 24] applied stabilized FEM to real river transport but focused on tidal and accidental-release scenarios within a single fixed channel geometry rather than systematically varying geometric complexity. In practice, rivers may include bends, width variations, and physical obstacles (e.g., rocks or structures) that alter local flow patterns and create more complex concentration distributions. Moreover, multiple pollutant sources can interact and generate overlapping plumes, further complicating the transport dynamics. Studies on advection-diffusion problems in irregular or more realistic settings highlight that domain characteristics significantly affect numerical transport behavior and pollutant distribution patterns [16]. Recent advancements in numerical modeling have increasingly emphasized the need to represent environmental flows in more realistic geometries and configurations. However, many existing advection-diffusion studies still focus on idealized straight channels, simplified boundary conditions, or single-source pollutant releases to maintain analytical or computational tractability. As a result, the combined effects of multiple pollutant sources, channel curvature, and internal obstacles are rarely investigated within a unified numerical framework. This gap motivates the need for a systematic comparative study that isolates and evaluates the role of geometric complexity in pollutant transport behavior.

Based on these considerations, this study aims to numerically investigate two-dimensional pollutant transport in rivers using the advection-diffusion equation solved with the Finite Element Method (FEM) under increasingly complex geometric and source configurations. Unlike many previous FEM-based studies that focus on simplified straight channels or single-source scenarios, this work explicitly integrates curved channels, multiple pollutant sources, physical obstacles, and irregular river geometries within a single comparative framework. Rather than proposing a new numerical scheme, the contribution of this study lies in providing a systematic, quantitatively benchmarked comparison of five geometric and source configurations within a single consistent FEM framework, using standardized transport indicators (peak concentration, plume width, and residence time) that allow direct cross-case comparison. This positioning provides a controlled numerical basis for comparing idealized and geometry-aware transport representations relevant to river water-quality analysis.

2. Methods

This study considers two-dimensional pollutant transport in a river flow. The pollutant is assumed to be dissolved in the fluid and transported by advection due to the river velocity field as well as by diffusion due to concentration gradients. The river is represented as a two-dimensional domain with geometries ranging from simple to complex, including a straight channel, a curved channel, a domain with internal obstacles, and an irregular domain. These variations are intended to evaluate the influence of physical geometry on pollutant-spreading patterns. In this study, the standard Galerkin formulation is employed without additional stabilization. The selected parameter range and mesh resolution yield qualitatively stable solutions for the scenarios investigated.

2.1. Finite Element Method (FEM) Formulation

To obtain numerical solutions of the two-dimensional advection-diffusion equation on river-like domains with curved boundaries and internal obstacles, this study employs the Finite Element Method (FEM), which is well suited for complex geometries and mixed boundary conditions.

Let $\Omega \subset \mathbb{R}^2$ denote the computational river domain with boundary $\partial\Omega$, and let $C(x, y, t)$ be the pollutant concentration. The governing advection-diffusion model can be written in non-conservative form as:

$$\frac{\partial C}{\partial t} + u\frac{\partial C}{\partial x} + v\frac{\partial C}{\partial y} = D\frac{\partial^2 C}{\partial x^2} + D\frac{\partial^2 C}{\partial y^2}. \tag{1}$$

Eq. (1) describes the temporal evolution of pollutant concentration as the combined effect of advection by the prescribed velocity components (u) and (v) and diffusion characterized by the coefficient (D). The prescribed velocity fields used to represent the different flow configurations are illustrated in Fig. 1 and determine the advective transport direction in Eq. (1). In this study, the diffusion coefficient is set to ($D = 0.001$).

In FEM, the weak (variational) form is derived by multiplying the PDE by a test function w and integrating over Ω. Applying integration by parts to the diffusion operator yields boundary integrals that naturally accommodate Neumann-type conditions, while Dirichlet conditions are enforced on prescribed boundaries. This standard Galerkin framework is widely described in FEM references for flow and transport problems [20].

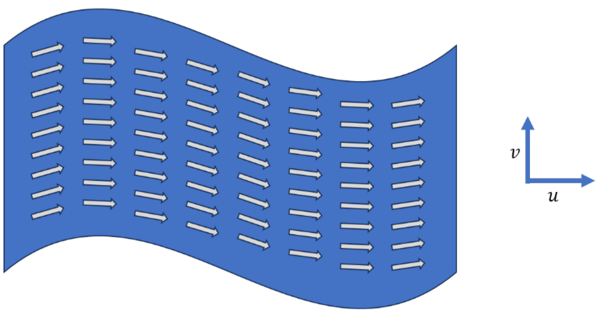

Fig. 1: Velocity fields in river stream

To accommodate irregular river geometries, the computational domain Ω is discretized into a conforming mesh of finite elements (e.g., triangles). The pollutant concentration is approximated by a piecewise-polynomial expansion given in Eq. (2).

$$C_h(x, y, t) = \sum_{i=1}^{n} c_i(t) N_i(x, y), \tag{2}$$

where N_i are Lagrange shape functions and $c_i(t)$ are nodal unknowns, which transforms the PDE into a semi-discrete system of ordinary differential equations (ODEs) given in Eq. (3).

$$\mathbf{M}\dot{c}(t) + (\mathbf{A} + \mathbf{K})\mathbf{c}(t) = \mathbf{f}(t), \tag{3}$$

with $\mathbf{M}$, $\mathbf{A}$, and $\mathbf{K}$ denoting the mass, advection, and diffusion matrices, respectively, and $\mathbf{f}$ the load vector associated with sources and boundary terms. This formulation is attractive for river-like domains because mesh resolution can be locally refined near bends, obstacles, and pollutant sources without requiring a structured grid.

For advection-dominated regimes (large Peclet numbers), the classical Galerkin method may produce spurious oscillations; therefore, many transport studies adopt stabilization schemes such as streamline upwind/Petrov-Galerkin (SUPG) to improve robustness without excessive numerical diffusion. These stabilized FEM approaches have been extensively analyzed for convection-diffusion(-reaction) problems and are known to improve robustness while preserving accuracy on complex geometries [25–28]. Stabilized FEM has been successfully used in two-dimensional advection-dispersion simulations for natural rivers, including tidal reaches and accidental mass-release scenarios, demonstrating its suitability for handling complex channel geometry, spatially varying flow fields, and sharp concentration gradients [23, 24].

2.2. Simulation Scenarios

Five scenarios are evaluated:

1. $u = 0.06$ m/s and $v = 0$ m/s with a single pollutant source;
2. u and v follow the domain (flow aligned with the river geometry);
3. $u = 0.06$ m/s and $v = 0$ m/s with two pollutant sources;
4. a domain containing rock obstacles with $u = 0.06$ m/s and $v = 0$ m/s;
5. an irregular river domain where u and v follow the domain geometry.

In this study, the velocity field is prescribed to isolate geometric effects on pollutant transport and enable consistent comparisons without added hydrodynamic complexity. Pollutant sources are modeled as localized Gaussian-like distributions to provide a simple and reproducible framework for plume evolution and obstacle interaction. The framework is therefore intended as a numerical testbed rather than a fully realistic river model and coupling with Navier-Stokes solvers and more realistic sources is left for future work.

The scenarios considered in this study are designed as idealized yet physically plausible representations of river transport conditions rather than site-specific simulations. The prescribed velocity magnitude is chosen within the typical range of slow-to-moderate river flow reported in environmental hydraulics literature, while the curved, obstacle-containing, and irregular domains are constructed to mimic commonly observed river features such as meanders, width variations, and submerged rocks. The goal is therefore to provide a controlled numerical environment that isolates geometric effects on pollutant transport, enabling systematic comparison across scenarios without the additional uncertainty introduced by field measurements.

2.3. Initial and Boundary Condition

For a single pollutant source, the initial condition and inflow condition at $x = 0$ are defined in Eq. (4).

$$IC = C(0, x, y) = 10 \exp\left(-\frac{(y-1)^2}{\sigma}\right) \exp\left(-\frac{x}{\varepsilon}\right), \tag{4}$$

with Dirichlet boundary condition:

$$C(t, 0, y) = 10 \exp(-\frac{(y-1)^2}{\sigma}).$$

For two pollutant sources, the initial condition is defined in Eq. (5).

$$IC = C(0, x, y) = 10 \exp\left(-\frac{(y-0.6)^2}{\sigma}\right) \exp\left(-\frac{x}{\varepsilon}\right) + 8 \exp\left(-\frac{(y-1.4)^2}{\sigma}\right) \exp\left(-\frac{x}{\varepsilon}\right), \quad (5)$$

with Dirichlet boundary condition of:

$$C(t, 0, y) = 10 \exp\left(-\frac{(y-0.6)^2}{\sigma}\right) + 8 \exp\left(-\frac{(y-1.4)^2}{\sigma}\right).$$

On other domain boundaries, Neumann conditions are applied for the wavy and irregular river domains. These conditions are given by $\partial C/\partial n = 0$ on the top and bottom boundaries and at the downstream boundary $x = L$, with the boundary locations following the corresponding domain geometry. On the riverbanks (top and bottom boundaries), the prescribed velocity field satisfies the no-penetration condition $u \cdot n = 0$ by construction.

$$\frac{\partial C}{\partial n} = 0 \text{ on } \begin{cases} y = y_c(x) + 1, \\ y = y_c(x) - 1, \end{cases} \quad \text{(top and bottom boundaries)}$$

$$\frac{\partial C}{\partial n} = 0 \text{ on } x = L \text{ (downstream boundary)}$$

For irregular stream domain:

$$\frac{\partial C}{\partial n} = 0 \text{ on } \begin{cases} y = y_c(x) + w(x), \\ y = y_c(x) - w(x), \end{cases} \quad \text{(top and bottom boundaries)}$$

$$\frac{\partial C}{\partial n} = 0 \text{ on } x = L \text{ (irregular-domain top and bottom boundaries)}$$

2.4. Numerical Implementation

All scenarios are simulated using Wolfram Mathematica 14.3 [29] using the FEM combined with the Method of Lines for time integration. The workflow includes constructing the computational domain, generating a triangular finite-element mesh, and solving the time-dependent system numerically using a Finite Element time integration.

Mesh generation is controlled through the parameter MaxCellMeasure, which is set to $h_{max} = 0.002$, providing sufficient spatial resolution to capture plume evolution around obstacles. Time integration is performed over $t \in [0, t_{max}]$, where $t_{max} = 150$ s for the wavy river domain and $t_{max} = 300$ s for the irregular river domain. The advection velocity magnitude is scaled by 0.06 m/s with spatially varying profiles derived from the river centerline and width, while the diffusion coefficients are fixed at $D_x = D_y = 0.001$. The velocity field $u(x, y)$ and $v(x, y)$ is prescribed as a function of spatial position only; it does not contain an explicit time-dependent term. As the prescribed velocity field is strictly steady, the velocity and concentration recorded at any fixed Eulerian point in the domain are expected to be time-invariant. The initial and inflow concentration fields are prescribed in Gaussian-type forms with parameters $\sigma = 0.5$ and $\varepsilon = 0.2$, representing localized pollutant releases. Inflow boundary conditions at $x = 0$ are imposed using Dirichlet constraints, while no-flux Neumann conditions are applied along the riverbanks.

For completeness, the following implementation details are provided for each scenario. The domain length and width vary by scenario, with a longer streamwise extent used for the irregular-domain case (Case 5) to accommodate its extended meandering path relative to the straight and moderately curved domains (Cases 1–4). The prescribed velocity field has a constant magnitude of 0.06 m/s in Cases 1, 3, and 4 ($u = 0.06$ m/s, $v = 0$), while in Cases 2 and 5 the velocity components $u(x, y)$ and $v(x, y)$ are constructed as smooth functions of the local channel centerline direction, so that the flow vector remains tangential to the centerline at each point and its magnitude is modulated by the local channel width (increasing in constricted sections and decreasing in widened sections). In Case 4, the rock obstacles are represented as circular regions excluded from the computational domain, with the prescribed velocity magnitude reduced within a neighborhood of each obstacle boundary to emulate local flow deceleration.

The numerical parameters used in this study were selected to balance computational cost and spatial resolution while preserving the qualitative transport features of the advection-diffusion process. The mesh resolution controlled by the MaxCellMeasure parameter was chosen to ensure sufficient refinement near pollutant sources, channel bends, and obstacle boundaries, where strong concentration gradients are expected.

Dirichlet boundary conditions are imposed at the inflow boundary to represent a prescribed upstream concentration, while homogeneous Neumann conditions are applied along riverbanks, where they represent zero total flux due to the no-penetration property of the prescribed velocity field, and along the downstream boundary ($x = L$), where $\partial C/\partial n = 0$ represents a zero-diffusive-flux open outflow condition, permitting advective transport of pollutant mass out of the domain. These assumptions are commonly used in idealized transport studies and allow the geometric effects on pollutant dispersion to be isolated. However, the simplified boundary conditions also imply that the model is intended as a controlled numerical testbed rather than a site-specific predictive model.

3. Results and Discussion

The results are presented progressively, beginning with the computational domain geometries and corresponding mesh structures, followed by the temporal evolution of pollutant concentration under the five simulation scenarios. The effects of flow configuration, source number, obstacles, and geometric complexity are then compared using both qualitative plume patterns and quantitative transport indicators. Finally, the computational discretization is examined to clarify how the numerical setup supports the interpretation of the simulated pollutant-transport behavior.

3.1. Domain Geometry

To facilitate interpretation of the numerical results, the characteristics of the computational domains used in each simulation scenario are first described. These domain geometries form the basis for understanding how flow structure and physical boundaries influence pollutant transport patterns.

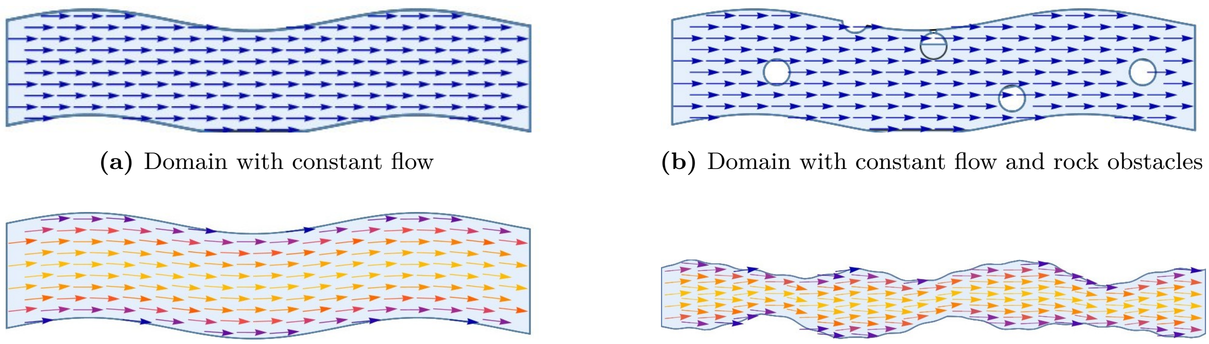

(a) Domain with constant flow

(b) Domain with constant flow and rock obstacles

(c) Domain with flow following the river path

(d) Irregular river domain

Fig. 2: Computational domain geometries used in the pollutant transport simulations

Fig. 2a represents a straight river with uniform width and no geometric disturbances. The velocity field is assumed constant, with horizontal component u and vertical component $v = 0$. In this case, advection primarily transports the pollutant downstream, while transverse spreading is due to diffusion. Fig. 2b shows a domain with constant flow and several rock obstacles that disturb the local flow. While the overall flow direction remains downstream, the obstacles are represented by locally modified velocity magnitudes in the prescribed field, producing regions of reduced flow speed near the rock boundaries. This prescribed deceleration is designed to approximate wake-like retention behavior typically associated with flow obstruction, without being physically derived from a solved flow model. Fig. 2c represents a gently curved river where the velocity components u and v vary spatially to follow the channel. The pollutant is transported downstream but also experiences lateral movement due to the nonzero v component, which can produce asymmetric plume shapes, especially near bends. Fig. 2d represents a more natural river geometry with significant width variation along the flow direction. Velocity magnitudes vary accordingly, increasing in constricted sections and decreasing in widened sections. This generates highly nonuniform transport and mixing patterns, producing more realistic and complex concentration distributions.

3.2. Domain Geometry and Mesh Structure

To ensure numerical stability and accuracy of the finite element solution, each computational domain is discretized using a triangular mesh adapted to the underlying geometry.

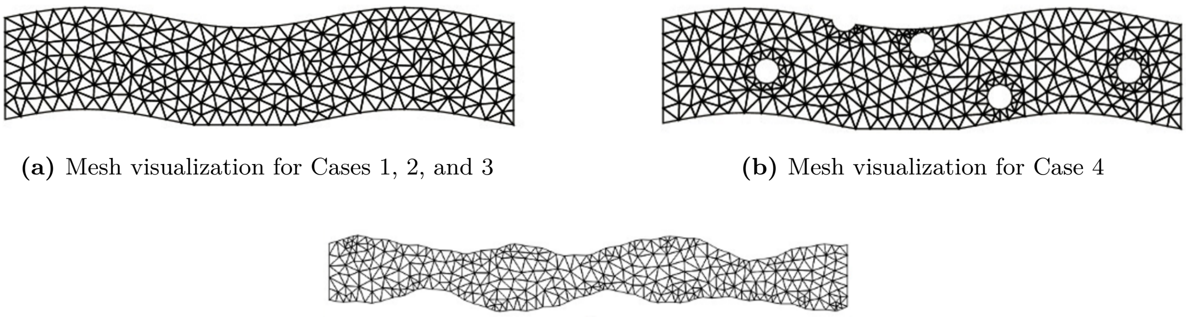

(a) Mesh visualization for Cases 1, 2, and 3

(b) Mesh visualization for Case 4

(c) Mesh visualization for Case 5

Fig. 3: Finite element mesh structures used in the pollutant transport simulations

Fig. 3a shows the finite-element mesh used for the first three scenarios, where the geometry variations are moderate. The triangular elements are relatively uniform across the domain, supporting stable and accurate FEM solutions. For Case 4 (Fig. 3b), the presence of circular rock obstacles requires local mesh refinement near obstacle boundaries. Smaller elements in these regions help capture sharp gradients in concentration and local changes in flow direction. Fig. 3c shows the mesh for the irregular river domain (Case 5). Element sizes vary adaptively to follow complex contours and width changes. Refinement in sharply curved or rapidly changing sections is important for representing solution gradients accurately.

3.3. Simulation Results

This subsection presents the numerical simulation results for all considered scenarios, highlighting the influence of flow conditions, domain geometry, physical obstacles, and the number of pollutant sources on two-dimensional pollutant dispersion. The temporal evolution of concentration fields is examined to illustrate how advection and diffusion interact under different river configurations.

Case 1: Constant flow ($u = 0.06$ m/s, $v = 0$) with a single pollutant source In Case 1 as shown in Fig. 4, at early times, the pollutant remains concentrated near the upstream release point, with only limited spreading due to diffusion. As time increases, steady downstream advection dominates the transport, producing a long, streamwise-oriented plume. The contours show gradual smoothing and mild transverse widening, indicating that diffusion mainly reduces sharp gradients while the plume motion is controlled by the uniform flow.

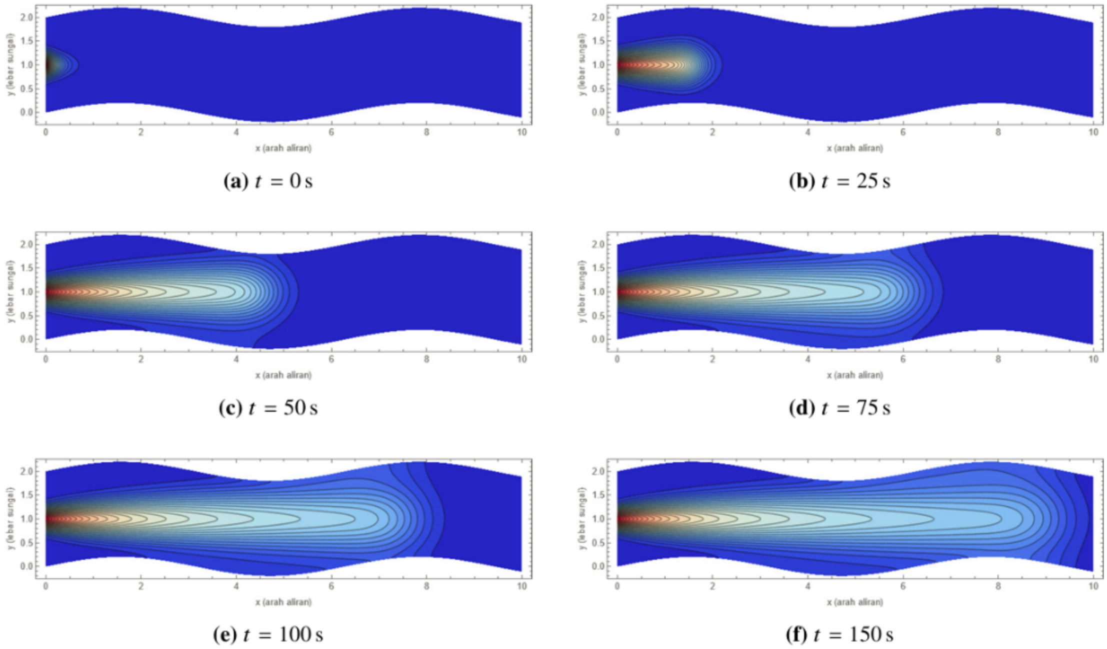

(a) $t = 0$ s (b) $t = 25$ s (c) $t = 50$ s (d) $t = 75$ s (e) $t = 100$ s (f) $t = 150$ s

Fig. 4: Pollutant dispersion in Case 1 (simple domain) from $t = 0$ to $t = 150$ s

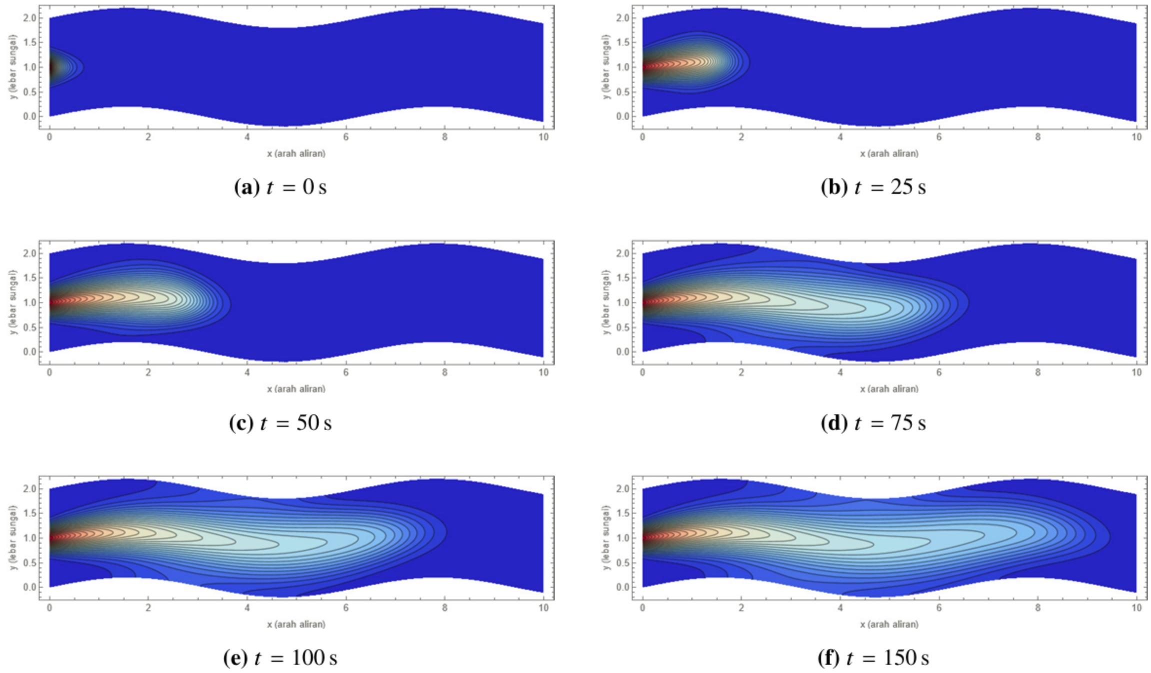

(a) $t = 0$ s (b) $t = 25$ s (c) $t = 50$ s (d) $t = 75$ s (e) $t = 100$ s (f) $t = 150$ s

Fig. 5: Pollutant dispersion in Case 2 (wavy river flow) from $t = 0$ to $t = 150$ s

Case 2: Geometry-following flow (u and v vary with the wavy channel) In this case, the plume does not travel as a straight downstream band (Fig. 5). Starting from $t = 50 - 75$ s, the concentration core shifts laterally and bends along the channel path, reflecting the influence of a nonzero transverse velocity component and local changes in flow direction. By $t = 150$ s, the plume becomes clearly asymmetric, showing that channel-following advection enhances plume deformation and produces more non-uniform mixing than constant-direction flow.

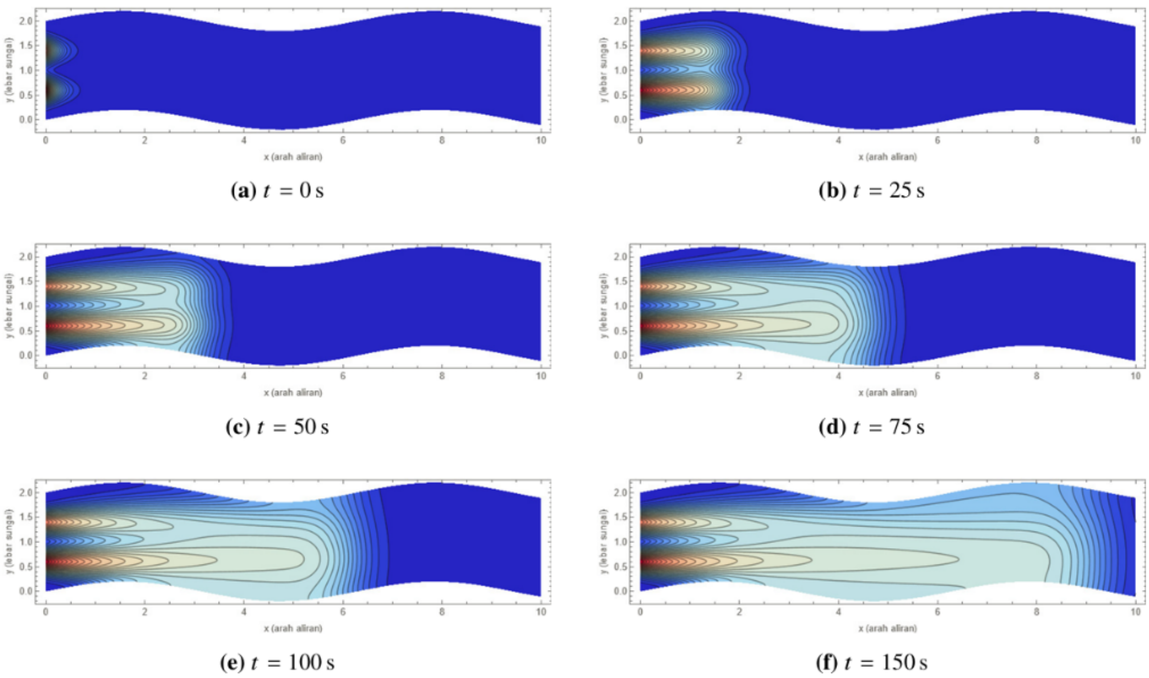

Fig. 6: Pollutant dispersion in Case 3 ($u = 0.06$ m/s, $v = 0$) from $t = 0$ to $t = 150$ s with two sources

Case 3: Constant flow ($u = 0.06$ m/s, $v = 0$) with two pollutant sources At $t = 0 - 25$ s, two separate high-concentration regions are visible at the release locations (Fig. 6). As advection carries both releases downstream ($t = 50 - 75$ s), two elongated plumes form and begin to interact. At later times ($t = 100 - 150$ s), the plumes overlap and merge into a wider combined plume, while peak concentrations decrease due to spreading and mixing.

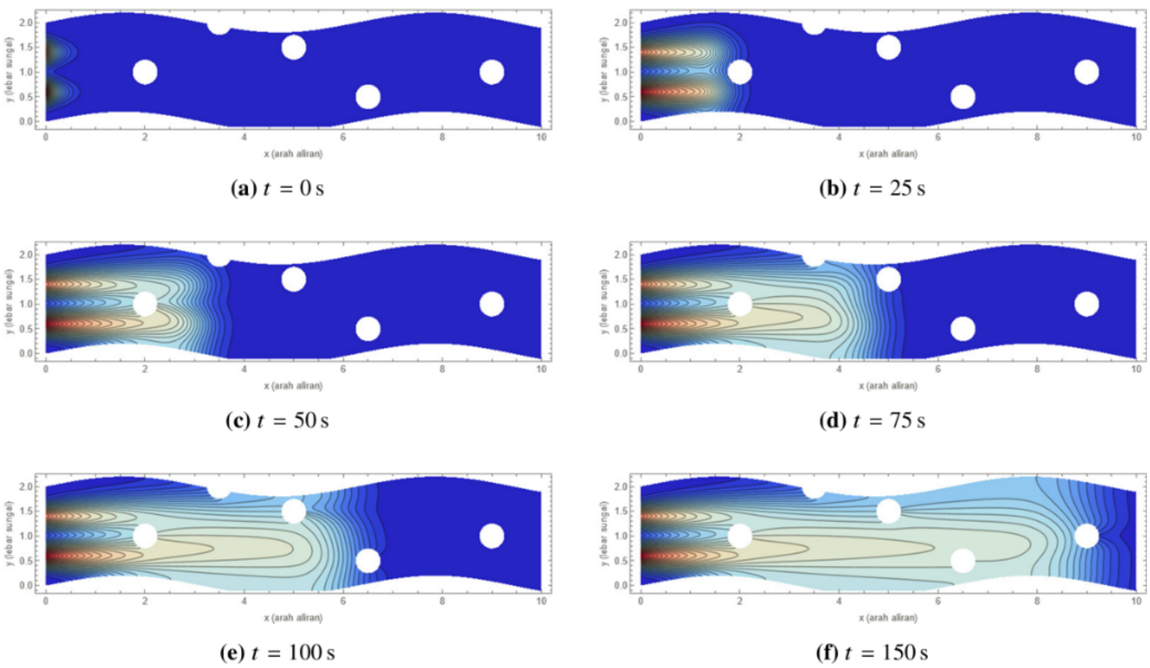

Fig. 7: Pollutant dispersion in Case 4 (flow with rock obstacles) from $t = 0$ to $t = 150$ s with two sources

Case 4: Constant flow with rock obstacles and two sources The obstacles significantly alter plume shape once the pollutant reaches them ($t \approx 50 - 75$ s) (Fig. 7). The concentration field splits and wraps around the rock boundaries, and the contours become distorted compared to the unobstructed case. Higher concentrations persist downstream in regions where the prescribe velocity field has locally reduced magnitude, consistent with the wake-like deceleration pattern built into the model, delaying transport and increasing spatial heterogeneity up to $t = 150$ s.

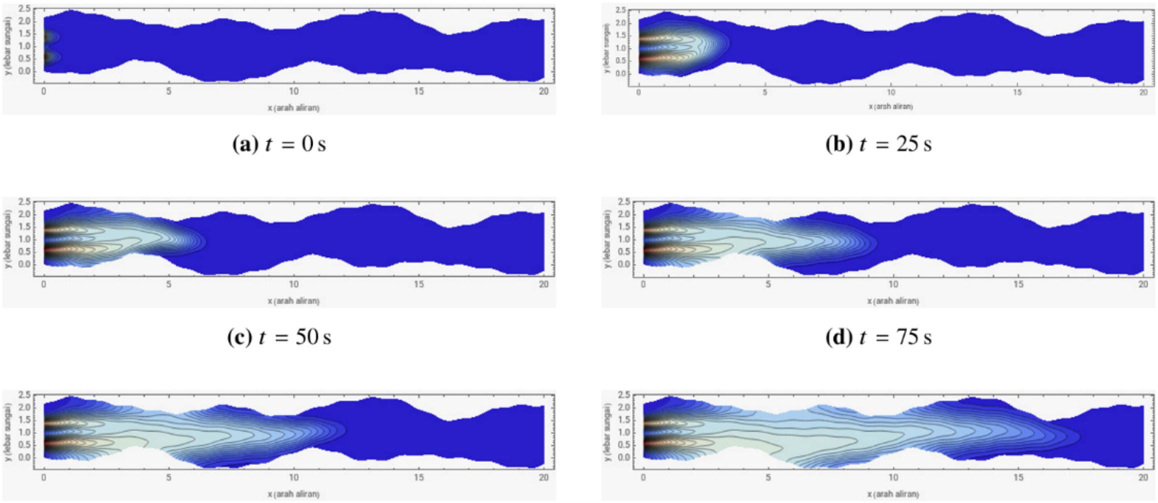

(a) $t = 0$ s **(b)** $t = 25$ s

(c) $t = 50$ s **(d)** $t = 75$ s

(e) $t = 100$ s **(f)** $t = 150$ s

Fig. 8: Pollutant dispersion in Case 5 (irregular domain) from $t = 0$ to $t = 150$ s with two sources

Case 5: Irregular river domain with geometry-following flow Case 5 exhibits the most complex behavior due to irregular geometry and variable width (Fig. 8). In constricted sections, increased velocity stretches the plume, whereas in widened sections, reduced velocity promotes lateral spreading and local accumulation. The combined effects of geometry-induced velocity variation and diffusion produce highly nonuniform and realistic concentration patterns.

3.4. Comparison Between Cases

This section compares plume behavior across the five simulated scenarios with different flow fields, source configurations, and geometric complexity. Differences in velocity structure, channel curvature, source number, and obstacles produce distinct concentration patterns in each case. It should be noted that Case 5 also differs from Cases 1-4 in domain length ($x \in [0, 20]$ versus $[0, 10]$) and simulation duration (300 s versus 150 s), so quantitative comparisons involving Case 5 reflect combined geometric, spatial, and temporal effects and not directly comparable in magnitude to Cases 1-4. These comparisons are intended to illustrate transport mechanisms under idealized conditions rather than to provide quantitatively validated predictions for real rivers. The present framework serves as a controlled numerical investigation of geometry-dependent transport behavior under prescribed flow and source conditions.

Case 1 (constant flow, one source) produces the simplest pattern: an elongated plume transported steadily downstream. Case 2 indicates that when the flow follows a curved channel, the plume deviates laterally and becomes asymmetric, emphasizing the role of channel geometry in setting the dominant transport direction. Case 3 demonstrates that multiple sources introduce plume-plume interaction and mixing. Diffusion gradually merges the two plumes into a wider distribution, creating more complex dynamics than the single-source case. Case 4 illustrates the effect of obstacles as represented in the prescribed flow field. The locally reduced velocity near the rocks produced slow-zone-like patterns, which lead to local accumulation and longer residence times within the model's assumptions. Case 5 is the most complex because width variations generate strong spatial variability in velocity. Plume stretching and widening occur in different regions, producing the most complex and illustrative dispersion patterns. These comparisons are intended to illustrate transport mechanisms under idealized conditions rather than to provide quantitatively validated predictions for real rivers.

In addition to visual comparison of concentration contours, the numerical results can also be interpreted through quantitative plume indicators. For instance, concentration profiles along selected cross-sections at fixed time instants reveal that plume width increases with geometric complexity, particularly in the irregular and obstacle-containing domains. The peak concentration decreases more rapidly in the two-source and irregular-domain scenarios due to enhanced mixing and plume interaction, while obstacle-induced retention zones produce locally elevated concentrations downstream. These observations provide a quantitative interpretation of the plume deformation and residence-time differences observed across the five cases.

To support the qualitative comparison above, Table 1 reports peak concentration, peak time, residence time, plume width plume area, and total pollutant mass for Cases 1-5.

Table 1: Quantitative transport indicators

Case	Peak Concentration	Peak Time (s)	Residence Time (s)	Plume Width	Plume Area	Total Mass
1	4.97390	106	122	1.04	16.2425	37.3713
2	4.83977	121	122	1.19	14.4625	35.2645
3	4.04777	100	122	1.99	18.8950	69.1487
4	4.83389	134	117	1.90	17.8475	67.0523
5	5.29683	300	275	1.50	30.2225	113.839

The highest peak concentration occurs in Case 1 (4.9739), reflecting the strongest local buildup under a single source in a straight channel. Case 3 shows the lowest peak concentration (4.04777), consistent with plume interaction between the two sources promoting earlier dilution despite the larger total pollutant load. Cases 2 and 4 show similar peak concentrations (around 4.84), suggesting that both channel curvature and the prescribed obstacle-related velocity reduction limit concentration build up through enhanced spreading. Regarding peak time, Case 3 reaches its maximum earliest (100 s) due to the simultaneous release from two sources, followed by Case 1 (106 s). The curved channel in Case 2 delays the peak to 121 s, and the latest peak occurs in Case 4 (134 s), consistent with the locally reduced velocity magnitude prescribed near the obstacles, which delays pollutant arrival at the observation point.

Residence time remains constant at 122 s for Cases 1–3, indicating that channel curvature and source number have limited influence on overall transport duration in this framework. Residence time decreases to 117 s in Case 4, consistent with the altered local velocity structure prescribed around the obstacles. Plume width increases from 1.04 in Case 1 to 1.19 in Case 2, consistent with lateral spreading induced by the curved channel geometry. The widest plumes occur in Cases 3 (1.99) and 4 (1.90), reflecting the combined effect of two pollutant sources and the obstacle-related velocity structure on transverse spreading. Plume area follows a similar pattern, with Case 2 showing the smallest value (14.4625) and Case 3 the largest (18.895), while Case 4 (17.8475) also shows substantial spreading consistent with the deformation of the plume around the prescribed obstacle geometry. Total pollutant mass is highest in Case 3 (69.1487), consistent with the additional source contributing roughly twice the pollutant load compared with single-source cases. Cases 1 and 2 show comparable total mass (37.3713 and 35.2645, respectively). Total mass in Case 4 (67.0523) is comparable in magnitude to Case 3 (69.1487), consistent with both scenarios releasing pollutant from two sources; the obstacle geometry in Case 4 redistributes the pollutant spatially rather than substantially altering the total injected mass. Case 5 shows the highest peak concentration (5.2968) and the largest plume area (30.2225) and total mass (113.839) among all cases. These values, however, are influenced not only by the irregular domain geometry but also by the longer simulation duration (t_{max} = 300s and 150s for Cases 1-4) and greater domain length, a direct magnitude comparison with Cases 1-4 should therefore be made with caution.

The numerical results also suggest that the qualitative transport patterns are broadly consistent across the parameter ranges explored during the simulation process, based on visual inspection of plume trajectories and deformation patterns under different mesh and diffusion-coefficient settings. However, a formal mesh-convergence and time-step sensitivity analysis was not conducted as part of this study and is identified as a limitation to be addressed in future work. Changes in the diffusion coefficient primarily affected plume width and smoothing without altering the dominant transport direction governed by advection.

Beyond numerical modeling, the results have practical implications for river water-quality management. The simulations indicate that channel curvature, width variation, and physical obstacles can significantly increase pollutant residence time and create localized accumulation zones. These findings suggest that river restoration and infrastructure planning should carefully consider how artificial structures, bank modifications, or channel engineering may unintentionally create pollutant retention regions. In pollution-control strategies, identifying slow-flow or recirculation-prone zones may help prioritize monitoring locations and optimize pollutant mitigation efforts.

The present study is subject to several limitations. The velocity field is prescribed rather than obtained from hydrodynamic simulations, and pollutant sources are represented using simplified Gaussian distributions. Additionally, the mesh is designed to capture qualitative plume behavior rather than achieve site-specific predictive accuracy. Consequently, the simulations are intended to provide a controlled comparative framework for understanding geometry-dependent transport mechanisms rather than direct predictions for a specific river system.

3.5. Computational Domain Discretization

Before any simulation can run, the river domain needs to be broken down into smaller, manageable pieces and that's exactly what this step does. The domain is divided using FEM (Fig. 9).

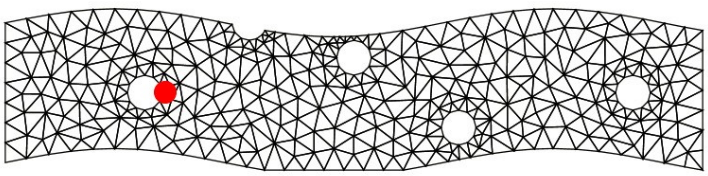

Fig. 9: Discretization of the computational domain using triangular finite elements (FEM). The red dot indicates the location of the observation point (2.3; 1.0). Mesh density is refined in the vicinity of the cylindrical obstacle

Triangles were chosen over rectangles for a simple reason: rivers aren't perfectly straight, and neither are cylindrical obstacles. Triangles handle those curves and irregular boundaries much better. Around the cylindrical obstacles specifically, the mesh is made finer and dense, because that's where flow changes the most dramatically over very short distances. Further away from the obstacles, where the flow is relatively calm and uniform, larger elements are used to keep computation efficient. The red dot at coordinate (2.3; 1.0) marks exactly where the velocity and concentration sensors are placed throughout the simulation.

4. Conclusion

The advection-diffusion equation provides an effective mathematical representation of pollutant spreading in river flows, and the Finite Element Method (FEM) enables stable numerical solutions on both simple and complex geometries. The comparative analysis across five scenarios demonstrates that flow velocity primarily governs plume direction and elongation, while diffusion smooths concentration gradients and widens the plume. More importantly, the study reveals that geometric complexity plays a decisive role in pollutant transport behavior. Channel curvature induces lateral plume deviation and asymmetry, multiple sources generate plume interaction and enhanced mixing, and the prescribed flow structure around obstacles produces localized regions of reduced velocity magnitude, which delay the peak arrival time of the pollutant plume (from 106 s to 134 s) and cause localized concentration accumulation, even though the residence time at the reference cross-section is slightly reduced (117 s versus 122 s in the unobstructured cases). In irregular domains, width variations lead to strong spatial variability in velocity, resulting in significantly deformed and non-uniform concentration patterns. These findings highlight that simplified straight-channel assumptions may underestimate local accumulation and plume deformation effects.

From a practical perspective, the results suggest that river geometry and infrastructure features should be carefully considered in water-quality management, as channel modifications or obstacles may unintentionally create pollutant retention zones. Future research may extend this framework by coupling the transport model with hydrodynamic solvers based on the Navier-Stokes equations, incorporating spatially varying velocity fields derived from field measurements, and validating the simulations using real river bathymetry and monitoring data. In addition, a rigorous quantitative validation of the numerical scheme — including mesh- and time-step convergence analysis and benchmarking against an analytical solution — should be conducted before the model is applied for predictive purposes. Such developments would enhance the predictive capability of geometry-aware pollutant transport modeling for real-world river systems.

CRediT Authorship Contribution Statement

Muhamad Adzka Rizkia: Conceptualization, Software, Visualization, Methodology, Writing-Original Draft. **Rahma Alya Zahrani:** Conceptualization, Formal Analysis, Writing-Original Draft, Writing-Review & Editing. **Zelisha Pitriatuz Zahra Fauzi:** Conceptualization, Methodology, Validation, Writing-Original Draft. **Foky Michelin:** Conceptualization, Writing-Original Draft. **Najwaa Alifya Azka:** Conceptualization, Writing-Original Draft. **Faiza Mayla Sabita:** Conceptualization, Writing-Original Draft. **Mualim Arya Ilyas Wiradinata:** Conceptualization, Writing-Original Draft. **Ferdy Aliansyah Hasyim:** Visualization, Writing-Review & Editing. **Mochamad Tito Julianto:** Supervision, Validation, Writing-Review & Editing. **Sri Nurdiati:** Supervision, Validation, Writing-Review & Editing. **Mohamad Khoirun Najib:** Supervision, Validation, Writing-Review & Editing. **Syukri Arif Rafhida:** Suvervision, Validation, Writing-Review & Editing.

Declaration of Generative AI and AI-assisted technologies

The authors used generative AI tools, such as Google Gemini 3 and ChatGPT, during the preparation of this manuscript. These tools were utilized to assist with language improvement, manuscript refinement, and support for Mathematica coding development. All outputs generated by these tools were carefully reviewed, verified, and edited by the authors.

Declaration of Competing Interest

The authors declare no competing interests.

Funding and Acknowledgments

This research received no external funding.

Data and Code Availability

The data and code supporting the findings of this study are available from the corresponding author upon reasonable request and subject to confidentiality agreements.

References

[1] Ellen Wohl. *Sustaining River Ecosystems and Water Resources*. Cham, Switzerland: Springer, 2017. DOI: doi.org/10.1007/978-3-319-65124-8.

[2] D. K. Petsch, V. de M. Cionek, S. M. Thomaz, and N. C. L. dos Santos. "Ecosystem services provided by river-floodplain ecosystems". In: *Hydrobiologia* 850.12–13 (2023), pp. 2563–2584. DOI: 10.1007/s10750-022-04916-7.

[3] M. C. Sousa, R. Martins, N. E. Simões, and M. J. Feio. "Ecosystem services of urban rivers: a systematic review". In: *Aquatic Sciences* 87.1 (2025). DOI: 10.1007/s00027-024-01138-y.

[4] A. Khosrovyan. "Biodiversity and ecosystem services in rivers". In: *Water* 16.15 (2024), p. 2091. DOI: 10.3390/w16152091.

[5] Widyarani, D. R. Wulan, U. Hamidah, A. Komarulzaman, R. T. Rosmalina, and N. Sintawardani. "Domestic wastewater in Indonesia: generation, characteristics and treatment". In: *Environmental Science and Pollution Research International* 29.22 (2022), pp. 32397–32414. DOI: 10.1007/s11356-022-19057-6.

[6] R. Wulandari et al. "Water pollution and sanitation in Indonesia: a review on water quality, health and environmental impacts, management, and future challenges". In: *Environmental Science and Pollution Research International* 31.58 (2024), pp. 65967–65992. DOI: 10.1007/s11356-024-35567-x.

[7] M. J. Luna Juncal, P. Masino, E. Bertone, and R. A. Stewart. "Towards nutrient neutrality: A review of agricultural runoff mitigation strategies and the development of a decision-making framework". In: *Science of The Total Environment* 874 (2023), p. 162408. DOI: 10.1016/j.scitotenv.2023.162408.

[8] N. Vita Hidayati et al. "Spatio - Temporal Distribution of Nitrate and Phosphate in Serayu Watershed, Central Java, Indonesia". In: *Jurnal Ilmiah Perikanan dan Kelautan* (2025). DOI: 10.20473/jipk.v17i3.72871.

[9] L. N. Fadlillah, S. Utami, A. A. Rachmawati, G. D. Jayanto, and M. Widyastuti. "Ecological risk and source identifications of heavy metals contamination in the water and surface sediments from anthropogenic impacts of urban river, Indonesia". In: *Heliyon* 9.4 (2023), e15485. DOI: 10.1016/j.heliyon.2023.e15485.

[10] G. Diansyah, Hermansyah, D. Rohendi, and T. Z. Ulqodry. "Risk assessment of heavy metal pollution in water, sediment, and fish from the Musi River Estuary, Indonesia". In: *Environmental Monitoring and Assessment* 197.9 (2025), p. 1051. DOI: 10.1007/s10661-025-14501-9.

[11] Pemerintah Republik Indonesia. *Peraturan Pemerintah Republik Indonesia Nomor 82 Tahun 2001 tentang Pengelolaan Kualitas Air dan Pengendalian Pencemaran Air*. Jakarta, Indonesia, 2001. https://peraturan.bpk.go.id/Details/53103/pp-no-82-tahun-2001.

[12] S. A. Rafhida, S. Nurdiati, R. Budiarti, and M. Khoirun Najib. "Bias correction of CMIP6 rainfall projection for the Lake Toba region, Indonesia, using quantile delta mapping with monthly distribution fitting". In: *Vietnam Journal of Earth Sciences* (2025). DOI: 10.15625/2615-9783/23833.

[13] S. N. Setyawati, S. Nurdiati, I. W. Mangku, I. Haidu, and M. K. Najib. "Time-varying bivariate modeling for predicting hydrometeorological trends in Jakarta using rainfall and air temperature data". In: *Hydrology* 12.10 (2025), p. 252. DOI: 10.3390/hydrology12100252.

[14] M. K. Najib et al. "Quantile mapping using the Alpha Power Transformed X-Lindley (APTXL) distribution for bias correction of Coupled Model Intercomparison Project Phase 6 (CMIP6) outputs: a case study over the Toba Lake region". In: *Theoretical and Applied Climatology* 157.1 (2026). DOI: 10.1007/s00704-025-05975-1.

[15] L. Sriwahyuni, S. Nurdiati, E. H. Nugrahani, and M. K. Najib. "Performance of machine learning for imputing missing daily rainfall data in east java under multiple satellite data models". In: *Geographia Technica* 20.1 (2025), pp. 346–368. DOI: 10.21163/gt_2025.201.23.

[16] G. Hutomo, J. Kusuma, and W. F. Zulfitri. "Solusi numerik menggunakan metode Dufort–Frankel pada persamaan adveksi–difusi 2D dengan koefisien variabel". In: *Axiomath: Jurnal Matematika dan Aplikasinya* 1.2 (2019), pp. 6–13. https://ejournals.umma.ac.id/index.php/axiomath/article/view/301.

[17] W. Strauss. *Partial Differential Equations: An Introduction*. 2nd ed. ISBN: 9780470054567. Hoboken, NJ, USA: John Wiley & Sons, 2009.

[18] J. Bear. *Dynamics of Fluids in Porous Media*. ISBN: 9780486656755. New York, NY, USA: American Elsevier, 1972.

[19] R. Szymkiewicz. *Numerical Modeling in Open Channel Hydraulics*. Cham, Switzerland: Springer, 2010. DOI: 10.1007/978-90-481-3674-2.

[20] J. Donea and A. Huerta. *Finite Element Methods for Flow Problems*. ISBN: 9780471496663. Chichester, U.K.: Wiley, 2003.

[21] J. N. Reddy and D. K. Gartling. *The Finite Element Method in Heat Transfer and Fluid Dynamics*. 3rd ed. ISBN: 9781420085983. Boca Raton, FL, USA: CRC Press, 2010.

[22] Alman. "Penyelesaian Numerik Persamaan Adveksi Difusi 2-D untuk Transportasi Polutan dengan Menggunakan Metode Beda Hingga Dufort Frankel". MA thesis. Makassar, Indonesia: Universitas Hasanuddin, 2013.

[23] M. E. Lee and I. W. Seo. "Analysis of pollutant transport in the Han River with tidal current using a 2D finite element model". In: *Journal of Hydro-environment Research* 1.1 (2007), pp. 30–42. DOI: 10.1016/j.jher.2007.04.006.

[24] M. E. Lee and I. W. Seo. "2D finite element pollutant transport model for accidental mass release in rivers". In: *KSCE Journal of Civil Engineering* 14 (2010), pp. 77–86. DOI: 10.1007/s12205-010-0077-9.

[25] A. N. Brooks and T. J. R. Hughes. "Streamline upwind/Petrov–Galerkin formulations for convection dominated flows with particular emphasis on the incompressible Navier–Stokes equations". In: *Computer Methods in Applied Mechanics and Engineering* 32.1–3 (1982), pp. 199–259. DOI: 10.1016/0045-7825(82)90071-8.

[26] L. P. Franca, S. L. Frey, and T. J. R. Hughes. "Stabilized finite element methods: I. Application to the advective–diffusive model". In: *Computer Methods in Applied Mechanics and Engineering* 95 (1992), pp. 253–276. DOI: 10.1016/0045-7825(92)90143-8.

[27] R. Codina. "On stabilized finite element methods for linear systems of convection–diffusion-reaction equations". In: *Computer Methods in Applied Mechanics and Engineering* 188.1–3 (2000), pp. 61–82. DOI: 10.1016/S0045-7825(00)00177-8.

[28] L. P. Franca, G. Hauke, and A. Masud. "Revisiting stabilized finite element methods for the advective–diffusive equation". In: *Computer Methods in Applied Mechanics and Engineering* 195 (2006), pp. 1560–1572. DOI: 10.1016/j.cma.2005.05.028.

[29] Wolfram Research, Inc. *Wolfram Mathematica, Version 14.3*. Champaign, IL, USA, 2025. https://www.wolfram.com/mathematica/quick-revision-history/.